EFFECT OF THE SHAPE OF METAL SOLIDS
ON THE RATE OF THEIR JOULE HEATING
IN ELECTROMAGNETIC RAIL LAUNCHERS

S. V. Stankevich and G. A. Shvetsov

This paper presents a method and results of numerical simulations of current-density, magnetic-field, and temperature distributions in rail launchers of conducting solids for armatures of various shapes. A comparison is made of the results of calculations using two-dimensional and three-dimensional models. It is shown that for cylindrical and saddle-shaped armatures, Joule heating calculations performed by two-dimensional simulation of electromagnetic and thermal phenomena are in good agreement with calculations for the three-dimensional model.

Key words: *electromagnetic rail launchers, metal armature, current density, Joule heating.*

Introduction. To reach high velocities in electromagnetic rail launchers (ERL) with a metal armature and to increase the service life of the launcher, it is necessary, as a rule, to maintain metal contact between the rails and armature throughout the acceleration process. Transition to arc contact is extremely undesirable since it reduces the acceleration, and leads to degradation of the launcher barrel and fracture of the projectiles.

The main mechanisms involved in the transition to arc contact are the loss of contact force, velocity skin effect (VSE), mechanical wear of the armature, armature fracture under the action of magnetic forces and magnetic cutting of the central part of the armature, electrodynamic unloading of the contact, etc. [1]. However, an analysis of papers (see, for example, [2]) shows that, in many cases, crisis processes leading to disruption of metal contact develop when the armature is heated to temperatures at which melting and (or) vaporization of the material begins.

To limit the heating of the launcher and projectile throughout the acceleration process, it is necessary to impose restrictions on the maximum magnetic field strength in the channel and, hence, on the maximum linear current density in the electromagnetic launcher. Obviously, if these conditions are satisfied, the velocity to which a solid of given mass can be accelerated on a given distance is also limited, and for homogeneous materials, its is, as a rule, of the order of 1 km/sec.

Previous calculations [2, 3] have shown that the ultimate (for heating conditions) characteristics of launchers depend largely on the electrothermal properties of the structural materials used, the kinematic parameters of the launcher, projectile mass, the acceleration dynamics determined by the shape of the current pulse, and the acceleration distance; these characteristics can be increased severalfold by using structural and composite conductors in the current-carrying units of launchers and by optimizing the current pulse shape. However, the results presented in [2, 3] and in a number of other papers have been obtained by numerical simulations of launchers in a two-dimensional formulation. The question of how much the maximum current density on the armature–rail interface, the armature heating rate, and the ultimate (for heating conditions) kinematic characteristics in real launchers differ from those obtained in two-dimensional simulation has not been solved. The purpose of the present work was to perform three-dimensional calculations and compare their results with the results of two-dimensional calculations of the heating of armatures of various shapes under identical acceleration dynamics and total current distributions.
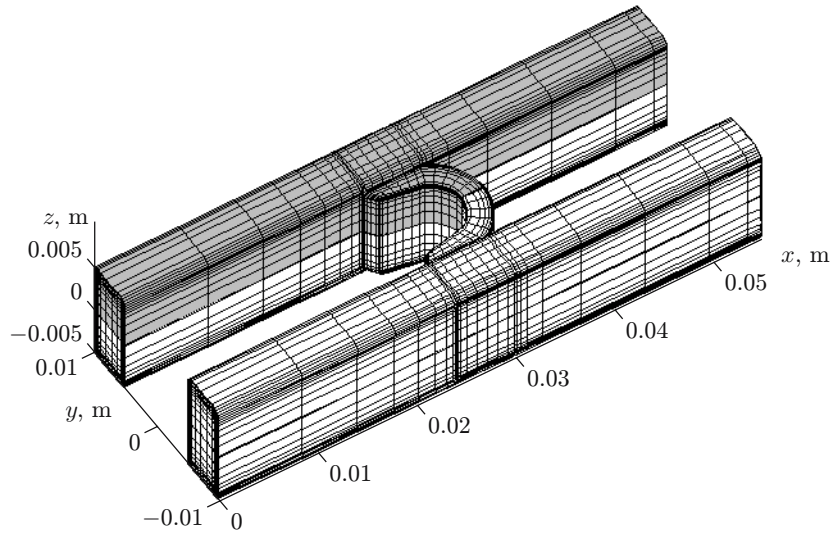
Fig. 1. Fragment of the rail launcher: the dark region is the calculation domain.

1. Formulation of the Problem. Complete modeling of rail launchers in a three-dimensional formulation requires lengthy calculations; therefore, in the present paper, we consider only a launcher armature and a fragment of the rails in immediate proximity to the armature (Fig. 1). Because of the symmetry of the electromagnetic launcher, the problem can be reduced to investigation of the electromagnetic and thermal processes occurring in one-quarter of the volume of the armature and rails (the dark region in Fig. 1).

The problem can be further simplified by taking into account that, even at low velocities of the armature (≈ 50 m/sec), currents flow in a thin surface layer at the armature–rail interface and their distribution is determined primarily by the shape of the armature and rails and by the armature velocity. To determine the current density distribution in the armature and rails near the interface, it is possible to ignore diffusion processes and use stationary solutions of the Maxwell equations. In addition, we assume that, during acceleration, ideal electrical and thermal contacts are maintained between the armature and rails and the electrothermal parameters of the materials remain constant (do not depend on temperature).

Ignoring bias currents and setting the magnetic permeability of the medium equal to the magnetic permeability of vacuum μ_0, from the Maxwell equations we obtain a system of equations for the vector and scalar potentials $(\boldsymbol{A}, \varphi)$; in the region occupied by the conductors (the armature and rails), this system can be written as

$$\boldsymbol{j} = -\frac{1}{\mu_0} \nabla^2 \boldsymbol{A} = -\sigma(\nabla\varphi - \boldsymbol{v} \times \nabla \times \boldsymbol{A}); \tag{1}$$

$$\nabla \cdot \boldsymbol{j} = \nabla \cdot (\sigma(\nabla\varphi - \boldsymbol{v} \times \nabla \times \boldsymbol{A})) = 0, \tag{2}$$

where σ is the electrical conductivity and $\boldsymbol{v}$ is the armature velocity. In the nonconducting space surrounding the conductors, where the current density $\boldsymbol{j} = 0$, instead of Eq. (1) we have

$$\nabla^2 \boldsymbol{A} = 0. \tag{3}$$

In the armature and rails, the temperature distribution $T(\boldsymbol{r}, t)$ is determined by solving the nonstationary heat-conduction equation

$$\rho c \frac{\partial T}{\partial t} - \nabla \cdot k \, \nabla T = \frac{\boldsymbol{j}^2}{\sigma}, \tag{4}$$

where ρ is the density, c is the heat capacity, and k is the thermal conductivity of the material.

The electromagnetic part of the problem contains one boundary condition: at an infinitely distant boundary, the vector-potential component should vanish. On the boundaries between the conductors and between the conductors and the surrounding nonconducting space, the continuity conditions for the components of the vector potential and their derivatives are satisfied.

343

Accounting for the symmetry of the ERL allows a number of additional conditions to be obtained [4]. In particular, on the boundary S_y through which the current flows (the section $y = 0$ in Fig. 1), the following conditions are satisfied:

$$j_x = j_z = A_x = A_z = \frac{\partial A_y}{\partial y} = \frac{\partial \varphi}{\partial x} = \frac{\partial \varphi}{\partial z} = 0. \tag{5}$$

The vanishing of the tangential derivatives of the scalar potential implies that the potential is constant on this boundary. We set $\varphi\big|_{y=0} = 0$.

On the symmetry boundary through which the current does not flow: $j_n = 0$ (the section $z = 0$ in Fig. 1), the following conditions are satisfied:

$$j_z = A_z = \frac{\partial A_x}{\partial z} = \frac{\partial A_y}{\partial z} = 0. \tag{6}$$

In this problem, the main difficulty is the formulation of the boundary conditions on the boundary S_x of intersection of the rail with the plane $x = 0$. Taking into account that, at distances from the armature equal to several calibers, the currents in the rails flow primarily along them, we can approximately set

$$j_y = j_z = 0. \tag{7}$$

Then, for the components of the vector potential on the boundary S_x, we obtain

$$A_y = A_z = \frac{\partial A_x}{\partial x} = 0. \tag{8}$$

The vanishing of the normal derivative of the x-component of the vector potential is not a consequence of assumptions (7) but is used as an additional condition. Due to the motion of the conducting medium through the boundary S_x, the scalar potential on this boundary does not have a constant value and its distribution needs to be calculated separately. From Eq. (2) and the adopted conditions (7), for the scalar potential on the boundary S_x we have

$$\frac{\partial \varphi}{\partial y} = v_x\left(\frac{\partial A_y}{\partial x} - \frac{\partial A_x}{\partial y}\right), \qquad \frac{\partial \varphi}{\partial z} = v_x\left(\frac{\partial A_z}{\partial x} - \frac{\partial A_x}{\partial z}\right). \tag{9}$$

Differentiating the first equation in (9) with respect to y and the second equation with respect to z, combining the resulting expressions, and taking into account the condition $\nabla \cdot \boldsymbol{A} = 0$, we obtain

$$\frac{\partial^2 \varphi}{\partial y^2} + \frac{\partial^2 \varphi}{\partial z^2} = v_x \frac{\partial}{\partial x}(\nabla \cdot \boldsymbol{A}) - v_x \nabla^2 A_x = -v_x \nabla^2 A_x = v_x j_x. \tag{10}$$

Equation (10) is satisfied on the plane of section of the rails S_x and supplements Eqs. (1)–(3).

Boundary conditions (5)–(10), the conditions of damping of the fields at infinity and the conditions of conjugation of the fields on the boundaries of the conductors are insufficient for obtaining a unique solution of the problem of calculating the potentials. To complete the formulation of the electromagnetic part of the problem, it is necessary to specify the value φ_0 of the scalar potential at any point on the boundary S_x. The value φ_0 should be chosen such that the calculated total current through the launcher corresponds to the given total current.

The boundary conditions for the heat-conduction equation (4) involve the requirement of the absence of heat exchange with the surrounding medium during acceleration and reduce to the Neumann boundary conditions on the outer boundaries of the conductors. On the contact boundary, the continuity condition for the temperature and normal heat-flux component (ideal thermal contact) was used.

2. Numerical Solution Procedure. In the conductors, Eqs. (1), (2), and (4) were approximated using the Galerkin weighted residual finite-element method [5], and outside the conductors, the boundary element method was employed [6]. For the two-dimensional case, this procedure is described in [7].

The region of the conductors is discretized by a finite-element grid. The vector and scalar potential fields in the conductors are approximated by means of functions of the form N_i ($i = 1, 2, \ldots, n$) and the nodal values of the vector and scalar potentials A_{pi} and φ_i:

$$A_p(\boldsymbol{r}) \approx N_{pi}(\boldsymbol{r})A_{pi}, \qquad \varphi(\boldsymbol{r}) \approx N_{fi}(\boldsymbol{r})\varphi_i \tag{11}$$

($p \in \{x, y, z\}$). Applying the weighted-residual method to Eqs. (1) and (2), we obtain a system of linear equations, which in matrix form is written as

344

$$KA_p - \sum_q V_{pq}A_q + D_p\varphi = B\frac{\partial A_p}{\partial n} \qquad \forall\, p \in \{x, y, z\}; \tag{12}$$

$$K_f\varphi - \sum_q V_{fq}A_q = \iint_{S_x} N_f j_x\, dS + \iint_{S_y} N_f j_y\, dS. \tag{13}$$

Here A_p and φ are discrete vectors whose components are the values of the corresponding variables at the nodal points of the finite-element mesh; n is the outward normal unit vector to the surface of the conductors; $q \in \{x, y, z\}$; $N_f = (N_{f1}, N_{f2}, \ldots, N_{fnp})^t$ is the vector of the basis functions; K, K_f, D_p, B, V_{pq}, and V_{fq} are matrices with the components

$$K_{ij} = \int_{\Omega_C} \nabla N_i \cdot \nabla N_j\, dV, \qquad K_{fij} = \int_{\Omega_C} \sigma \nabla N_i \cdot \nabla N_j\, dV, \qquad D_{pij} = \int_{\Omega_C} \sigma N_{pi} \frac{\partial N_{fj}}{\partial p}\, dV,$$

$$B_{ij} = \int_{S_{NC}} N_i N_j\, dS, \qquad V_{pqij} = \int_{\Omega_R} \sigma N_{pi}\left(v_q \frac{\partial N_{qj}}{\partial p} - v \cdot \nabla N_{qj}\right) dV,$$

$$V_{fqij} = \int_{\Omega_R} \sigma\left(v_q \nabla N_{fi} \cdot \nabla N_{qj} - \frac{\partial N_{fi}}{\partial q} v \cdot \nabla N_{qj}\right) dV,$$

where Ω_C is the region of the conductors (rails and armature), Ω_R is the region of the rails, and S_{NC} is the boundary between the conductors and the surrounding space.

Equations (12) and (13) contain unknown values of the normal derivatives of the vector potential components on the boundary S_{NC} and the j_x- and j_y-components of the current density on the boundary S_x and S_y.

Using the Green formula and applying the weighted-residual method to Eq. (3) with the weight function which is the fundamental solution of (3), we calculate the normal derivatives of the magnetic potential vector components. As a result, for each node i on the boundary S_{NC}, we obtain the integral equation

$$\frac{\beta_i}{4\pi} A_{pi} + \int_{S_{NC}} \left(A_p \frac{\partial \psi_i^*}{\partial n} - \psi_i^* \frac{\partial A_p}{\partial n}\right) dS = 0, \tag{14}$$

where $\psi_i^* = (4\pi|r_i - r|)^{-1}$ is the fundamental solution; the coefficient β_i is equal to the exterior solid angle of the boundary at the boundary node r_i. The boundary S_{NC} is partitioned into boundary elements so that they coincide with the edges of the volume finite-element mesh. The components of the vector potential and their normal derivatives on the boundaries are interpolated similarly to (11). Calculating (14) at each boundary node, we obtain

$$HA_p = Q\frac{\partial A_p}{\partial n}, \tag{15}$$

where H and Q are matrices with the components

$$H_{ij} = \frac{\delta_{ij}\beta_i}{4\pi} + \int_{S_{NC}} \frac{\partial \psi_i^*}{\partial n} N_{pj}\, dS, \qquad Q_{ij} = \int_{S_{NC}} \psi_i^* N_{pj}\, dS,$$

and δ_{ij} is the Kronecker delta. From the system of linear equations (15), it is possible to find the values of the normal derivatives of the vector potential components at the nodes on the boundaries of the conductors:

$$\left.\frac{\partial A_p}{\partial n}\right|_{S_{NC}} = -Q^{-1}HA_p\Big|_{S_{NC}}. \tag{16}$$

Here the minus sign indicates that the outward normal direction for the conducting subregions is opposite to the to normal direction on the outer boundaries of the nonconducting space. Substitution of expression (16) into Eq. (12) yields

$$(K + K')A_p - V_{pq}A_q + D_p\varphi = 0,$$

where $K' = BQ^{-1}H$ is a matrix.

As noted above, the equations containing the unknown current densities on the boundary S_y can be eliminated from system (12), (13) since on this boundary, zero potential is assumed. The unknown current density on the boundary S_x can be eliminated using expression (10). Substituting (10) into the right side of (13) and performing integration by parts, we obtain

$$\int\limits_{S_x} \boldsymbol{N}_f j_x \, dS = -v_x^{-1} \int\limits_{S_x} \left(\frac{\partial \boldsymbol{N}_f}{\partial y} \frac{\partial \varphi}{\partial y} + \frac{\partial \boldsymbol{N}_f}{\partial z} \frac{\partial \varphi}{\partial z} \right) dS + v_x^{-1} \oint\limits_{\partial S_x} \boldsymbol{N}_f \frac{\partial \varphi}{\partial \boldsymbol{n}} \, dL.$$

Here the normal vector $\boldsymbol{n}$ is in the plane $x = 0$ and is perpendicular to the curve bounding the section of the rails by this plane. We note that, at almost each point of this curve, the direction of the vector $\boldsymbol{n}$ coincides with the direction of the normal to the boundary S_{NC}. Using relations (9), we calculate the normal derivative of the potential:

$$\frac{\partial \varphi}{\partial \boldsymbol{n}} = v_x \left(\frac{\partial A_x}{\partial \boldsymbol{n}} - n_y \frac{\partial A_y}{\partial x} - n_z \frac{\partial A_z}{\partial x} \right). \tag{17}$$

The derivatives $\partial A_x / \partial \boldsymbol{n}$ in expression (17) can be obtained from Eq. (16), whereas the derivatives of the potential components parallel to the boundary plane S_x should be calculated on the basis of approximation (11).

Let us discretize the calculation domain (see Fig. 1) by a nonuniform finite-element mesh of hexagonal elements. The potentials are approximated by linear basis functions. Since the mesh has the following typical parameters: ≈ 5500 volume elements, ≈ 2000 surface elements, and ≈ 6500 calculation points, it is necessary to solve a system of equations with approximately 26,000 unknowns. The system of linear equations was solved by a direct method. In the calculations, the maximum armature velocity was approximately 500 m/sec. To obtain the solution for high velocities of armature motion, it is necessary to use a finer mesh (which is difficult with the available computer memory size) or to increase the order of element approximation.

Because of the stationarity of the electromagnetic part, the solution of the problem can be divided into solution of the electromagnetic problem and solution of the thermal problem. As a first stage, it is possible to solve problem (1)–(3) and find the current density distributions in the armature and rails and the accelerating magnetic pressure forces F_i for a certain set of armature velocities v_i; as a second stage, the armature heating problem (4) is solved with the right side of Eq. (4) containing the time dependence of the current density obtained by interpolation over known values of the function $\boldsymbol{j}(\boldsymbol{r}, v_i)$. Time dependences of the armature velocity and current density distribution are calculated by integration of the equation of motion $m\dot{v} = F_i$ (m is the total mass of the armature).

For comparison of the three-dimensional and two-dimensional simulation results, the problem of rail launcher heating was solved in a two-dimensional formulation. The geometry of the computation domain was the midsection of a three-dimensional launcher (plane $z = 0$ in Fig. 1). The magnetic field magnitude in the launcher channel was set equal to the current density I/b (b is the rail width). In the two-dimensional formulation, we used the time dependence of the armature velocity obtained in three-dimensional calculations. For convenience of comparison with the three-dimensional simulation results, the two-dimensional problem was also solved in two stages: current density distributions versus armature velocity were first calculated, and the nonstationary thermal problem was then solved.

3. Calculation Results. In the first stage, the current density and magnetic field distributions, accelerating magnetic force, and inductance per unit length per unit length were calculated for an electromagnetic rail launcher with a channel cross section of 11×1 cm and copper rails 1.50 and 1.16 cm wide and 0.5 cm thick (see Fig. 1). To examine the effect of the armature shape and its electrothermal properties on the current density distribution, heating dynamics, and inductance gradient, we considered copper and aluminum armatures of various shapes: rectangular, C-shaped, cylindrical, rounded-edge C-shaped, and saddle-shaped armatures (Fig. 2).

Curves of the inductance per unit length versus armature velocity for copper armatures of various shapes are presented in Fig. 3. It is evident that the inductance per unit length is maximal for the C-shaped armature (see Fig. 2b). For all armature shapes, the inductance per unit length differ by not more than 10%. As the armature velocity increases, the inductance per unit length decreases due to current redistributions in the armature and rails. In the velocity range studied, the inductance per unit length decreases by approximately 5–10% and is almost identical for copper and aluminum armatures.

In the calculations, the maximum current density was reached on the boundary of the rail–armature interface. This is due, first, to the geometrical singularity at the interface between the lateral surface of the armature and the
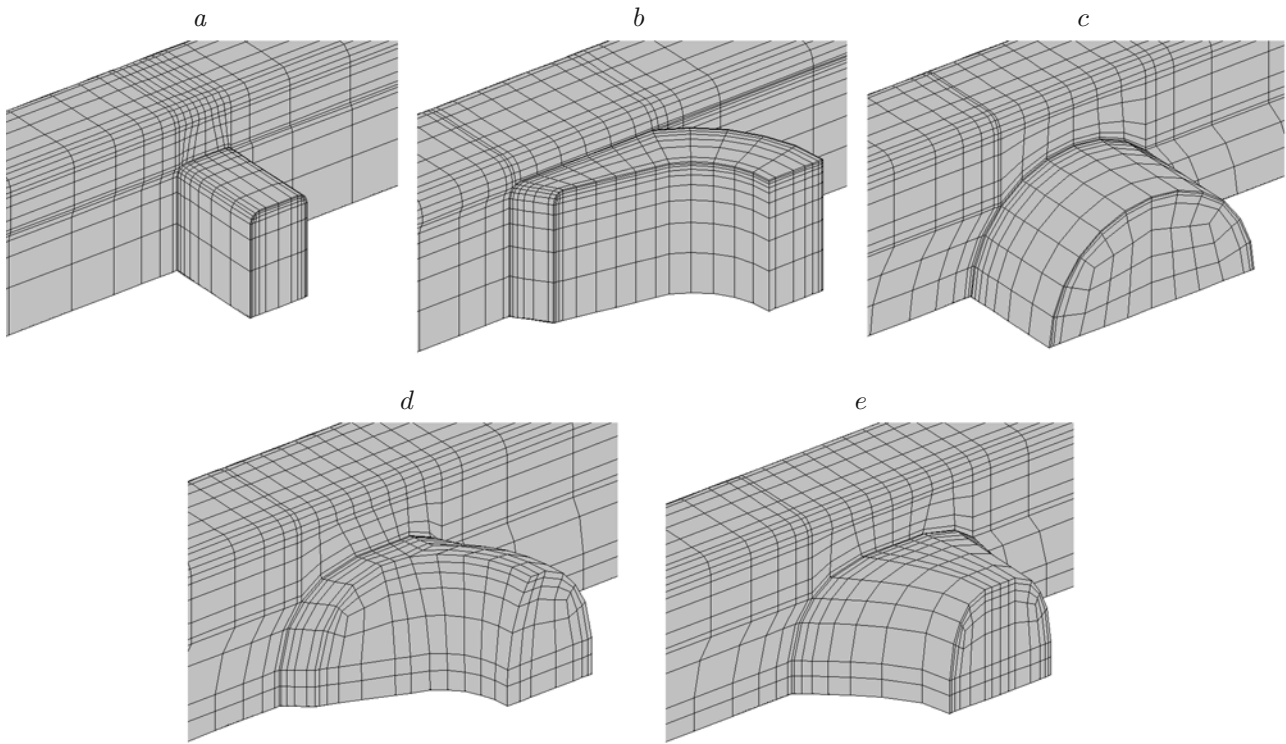
346

Fig. 2. Armature shapes: rectangular (a), standard C-shaped (b), cylindrical (c), rounded-edge C-shaped (d), and saddle-shaped (e).
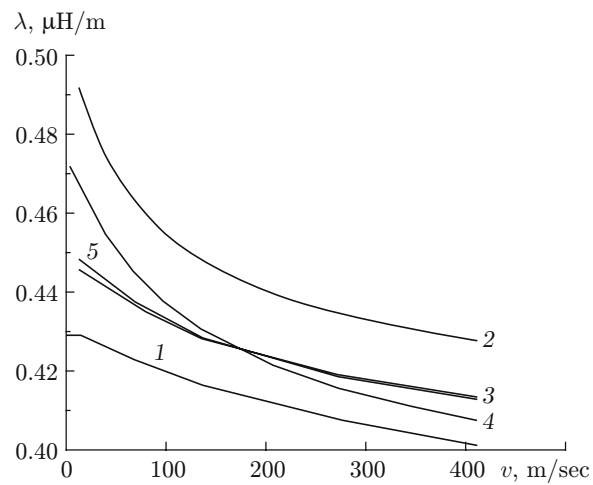

Fig. 3. Inductance per unit length versus armature velocity for copper armatures of various shapes: rectangular (1), C-shaped (2), cylindrical (3), rounded-edge C-shaped (4), and saddle-shaped (5).
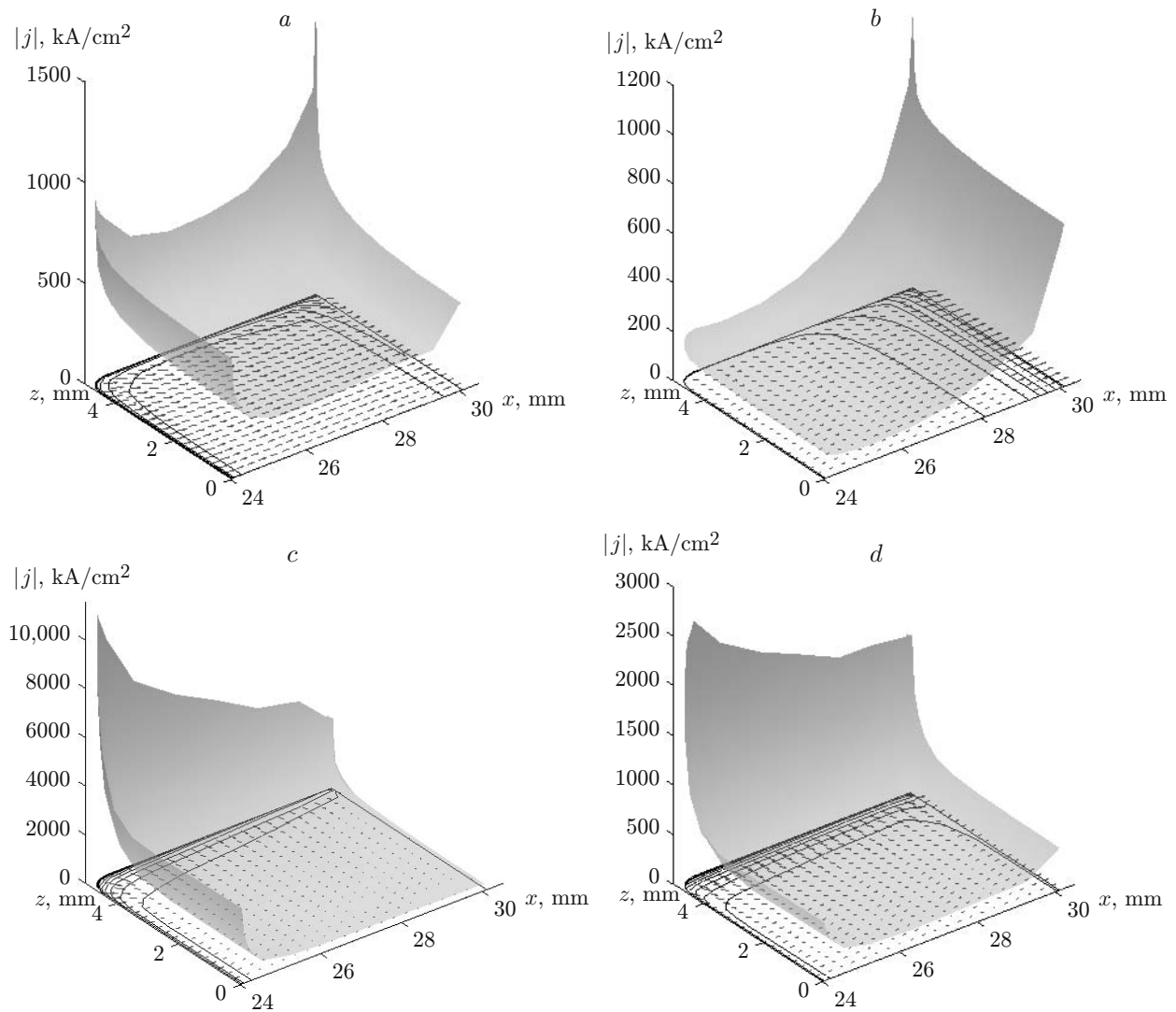
347

Fig. 4. Distributions of the current density modulus on the interface for standard C-shaped copper (a and c) and aluminum armatures (b and d) at various armature velocities: $v = 100$ (a and b) and 400 m/sec (c and d).

rail surface [8]; second, this is due to the VSE which draws the current to the rear part of the interface. The position of the point at which the absolute current density reaches the maximum value depends on the armature shape, its electrical conductivity, and motion velocity. This point can be located on the frontal, rear or another part of the interface. We note that, for rectangular and cylindrical armature, the current density maximum point is always on the rear part of the interface regardless of the material. As the armature velocity increases and the VSE is enhanced, the current density maximum point is shifted along the interface boundary to the rear part of the armature, despite the fact that, initially, this point can be located on the frontal part of the interface. This process is characteristic for armatures of all shapes studied. The armature velocity at which this shift occurs depends on the electrical conductivity of the armature. For armatures of identical shape, the shift of the current density maximum point for an armature with lower electrical conductivity occurs at higher velocity. Figure 4 shows distributions of the current density modulus on the interface for standard C-shaped copper and aluminum armatures at velocities $v = 100$ and 400 m/sec. We note that the calculated current densities presented in Fig. 4 depend greatly on the characteristic sizes of the elements used in the finite-element approximation of Eqs. (1) and (2). These distributions are mainly qualitative (although they were obtained for almost identical characteristic element sizes) and indicate nonuniform current distribution.
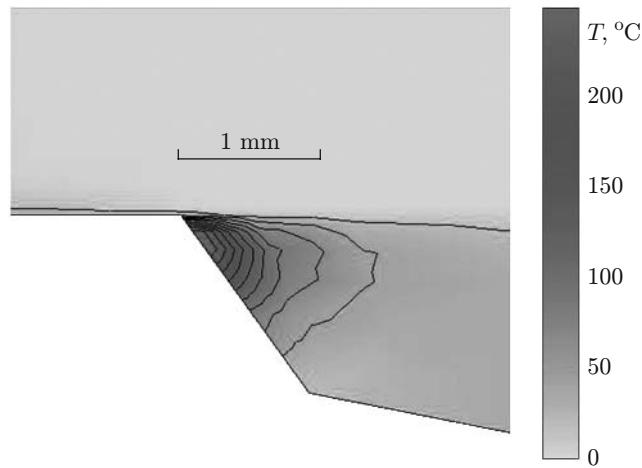
348

Fig. 5. Temperature distribution in the C-shaped copper armature at the time corresponding to motion velocity $v = 200$ m/sec.
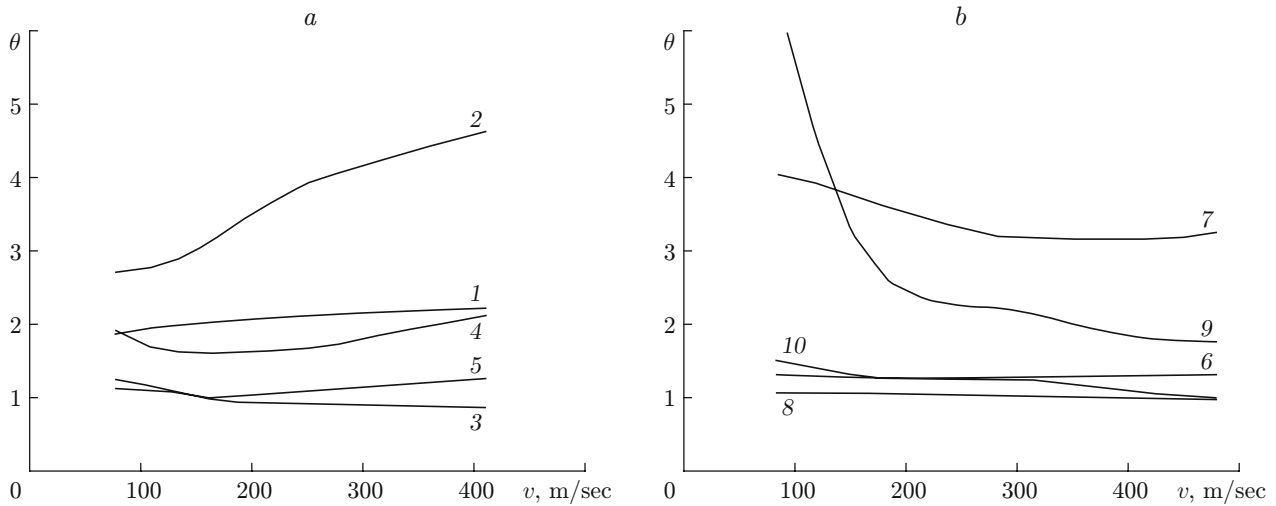

Fig. 6. Ratios of the maximum temperatures calculated in the three-and two-dimensional formulations versus velocity for copper armature (a) and aluminum armature (b) of various shapes and masses: rectangular armature with $m = 2.66$ (1) and 0.82 g (6), C-shaped armature with $m = 3.54$ (2) and 1.08 g (7),cylindrical armature with $m = 6.95$ (3) and 2.13 g (8), rounded-edge C-shaped armature with $m = 4.13$ (4) and 1.27 g (9), and saddle armature with $m = 5.43$ (5) and 1.67 g (10).

In the calculation of the current density distribution in the armature in the two-dimensional formulation with the adopted boundary conditions, the current density reaches the maximum on the line of contact between the rear surface of the armature and the rail surface. Thus, the two-dimensional model is not suitable for correctly calculating current density distributions for armatures (in particular, for C-shaped armatures) in which the maximum current density is reached (in a certain velocity range) in the frontal part of the interface. However, by modifying the shape of such an armature or by rounding its leg (the terminology of [9]) and the frontal surface (Fig. 2d), it is possible to reach a more uniform current density distribution along the interface boundary and a shift of the current density maxima to the rear part of the interface at a velocity $v = 100$ m/sec for the copper armature and $v = 200$ m/sec for the aluminum armature. Prospects for using saddle-shaped armatures are considered in [9, 10]. In the present work, for an armature of this type (see Fig. 2e) (somewhat different in shape from the armatures considered in [9, 10]), calculations were performed and, indeed, a more uniform current density distribution along the interface boundary was obtained.
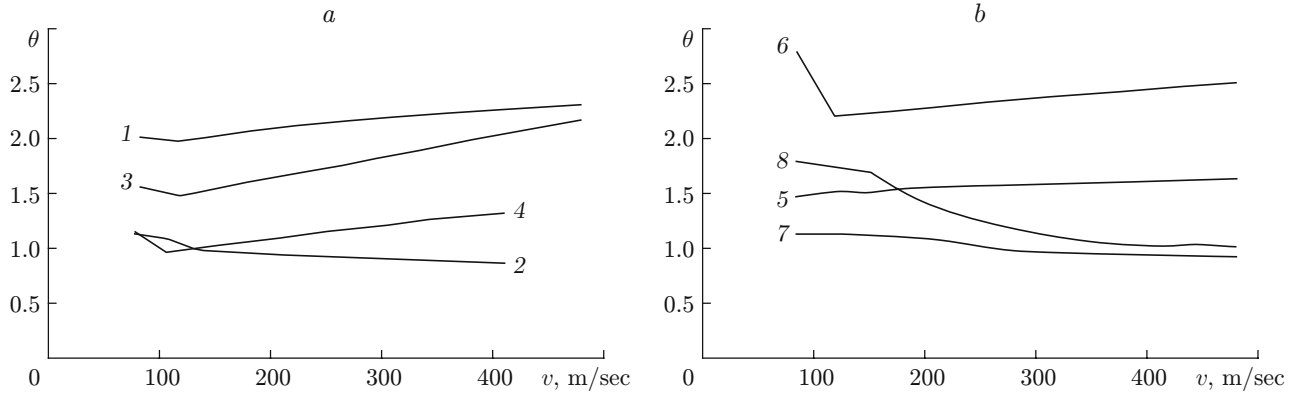
349

Fig. 7. Ratios of the maximum temperatures calculated in the three-and two-dimensional formulations versus motion velocity for copper armatures with $m = 10$ g (a) and aluminum armatures with $m = 5$ g (b) of various shapes: rectangular (1 and 5), cylindrical (2 and 6), rounded-edge C-shaped (3), C-shaped (7), and saddle-shaped (4 and 8).

In the second stage, using the procedure described above, we calculated the nonstationary temperature distribution in the armature. It was assumed that the armature was accelerated in the rail launcher at a total constant current equal to 100 kA. It was found that the position of the region (point) in which the temperature maximum is reached during armature acceleration can differ significantly from the position of the point at which the current density is maximal. This is due to heat removal from the region of current concentration to neighboring regions of the armature due to thermal conductivity. This effect is most characteristic of the interface boundary, which is continuously cooled due to the displacement of the armature to the cold regions of the rails. At projectile velocities of the order of 200 m/sec, the rail surface temperature on the interface is almost identical to the initial temperature.

Figure 5 shows the temperature distribution near the line of contact between the rear surface of the C-shaped copper armature and the rails for motion velocities $v = 200$ m/sec. Heat transfer by thermal conduction from the regions with the maximum current density slows down the heating in these regions. As a result, the temperature can reach the maximum value in regions with much lower current density away from the contact interface, in particular, in the middle part of the rear surface of the armature. However, as the armature is accelerated, the region of maximum heating is shifted from the middle part of the armature to the rear part of the interface boundary. This position of the region of maximum heating is observed in the initial stages of acceleration ($v < 100$ m/sec) for standard C-shaped, saddle-shaped armatures, and rounded-edge C-shaped copper armatures. For aluminum armatures of the same type, depending on the mass of the projectile package, the temperature can remain maximal at the centre of the armature throat throughout the acceleration process before reaching the maximum velocity $v = 500$ m/sec adopted in the calculations.

For armatures of all types, the heating rate depends on the acceleration of the armature. At a low acceleration (especially in the case where the maximum temperature is determined by the current concentration on the interface) the heating rate is lower, but in acceleration to same velocity, the maximum temperature increases approximately proportionally to the increase in the acceleration time.

Figure 6 shows curves of the ratios of the maximum temperature versus velocity calculated in three- and two-dimensional formulations $[\theta(v) = \max_{r} T_{3D}(r, v) / \max_{r} T_{2D}(r, v)]$ for copper and aluminum armatures of various shapes and masses. Figure 7 gives curves of the ratios of the maximum temperatures versus velocity calculated for copper and aluminum armatures of various shapes and the same total projectile mass $m = 10$ and 5 g, respectively. It is evident that for almost all armature shapes (except for the cylindrical copper armature), $\theta(v) > 1$. The ratios of the maximum armature temperatures calculated in the three-dimensional and two-dimensional formulations depend insignificantly on the armature velocity, especially at high motion velocities. The value of this ratio is determined primarily by the armature shape. A significant difference between the results of three-dimensional and two-dimensional calculations of the maximum temperature is observed for the C-shaped armature (see Fig. 5) and

350

the rounded-edge C-shaped armature (see Fig. 6). This is due to the fact that, in these cases, the region of maximum heating at low velocities is located in the frontal part of the interface and is not described in the two-dimensional simulation. For cylindrical and saddle-shaped armatures, the temperatures ratio $\theta(v) \to 1$.

Conclusions. The calculations performed in the present work do not allow wide generalization but the results show that two-dimensional calculations give upper-bound estimates for the ultimate velocities that can be attained in launchers providing limited armature heating during acceleration. For more exact two-dimensional simulations of various phenomena and processes in the launcher, it is possible to use the results of relatively simple three-dimensional calculations of the inductance gradient and the correction factor for the armature heating rate; in this case, the armature shape should be chosen so as to ensure the maximally uniform distribution of the current density along the interface boundary.

From the analysis of the results it follows that, for certain armature geometries (in the case considered, cylindrical and saddle-shaped armatures), the two-dimensional description of armature heating is in good agreement with its three-dimensional description. The calculation results suggest that a severalfold increase in the ultimate (for heating conditions) kinematic characteristics (shown by two-dimensional simulation in [2, 3]) is possible for real rail launchers of conducting solids.

REFERENCES

1. J. P. Barber, D. P. Bauer, K. Jamison, et al., "A survey of armature transition mechanisms," *IEEE Trans. Magn.*, **39**, No. 1, Part 1, 47–51 (2003).
2. S. V. Stankevich and G. A. Shvetsov, "Analysis of the ultimate kinematic characteristics of railgun launchers of solids," *J. Appl. Mech. Tech. Phys.*, **40**, No. 2, 325–330 (1999).
3. G. A. Shvetsov and S. V. Stankevich, "Search of new possibilities for attaining high launching velocities," *IEEE Trans. Magn.*, **37**, No. 1, 275–279 (2001).
4. D. Kondrashov and D. A. Keefer, "Maxwell equation solver for 3-D MHD calculations," *IEEE Trans. Magn.*, **33**, No. 1, 254–259 (1997).
5. K. Fletcher, *Computational Galerkin Methods*, Springer Verlag (1984).
6. Q. Chen and A. Konrad, "A review of finite element open boundary techniques and quasi-static electromagnetic field," *IEEE Trans. Magn.*, **33**, No. 1, Part 2, 663–676 (1997).
7. S. V. Stankevich, "Calculation of magnetic fields and currents in axially symmetric systems of inductively coupled moving conductors," *J. Appl. Mech. Tech. Phys.*, **50**, No. 1, 18–24 (2009).
8. M. P. Galanin and V. V. Savichev, "Singularities of electromagnetic fields and their manifestations in modeling electrical contact in electromagnetic rail launchers," *Teplofiz. Vysok. Temp.*, **35**, No. 4, 517–523 (1997).
9. L. Rip, S. Satapathy, and K.-T. Hsieh, "Effect of geometry change on the current density distribution in C-shaped armatures," *IEEE Trans. Magn.*, **39**, No. 1, Part 1, 72–75 (2003).
10. S. Satapathy, T. Watt, and Ch. Persad, "Effect of geometry change on armature behavior," *IEEE Trans. Magn.*, **43**, No. 1, 408–412 (2007).